PHYSICAL REVIEW C VOLUME 16, NUMBER 2 AUGUST 1977

Comparison of light- and heavy-ion emission from the $^{12}C + ^{16}O$ system*

S. L. Tabor, Y. Eisen,† D. G. Kovar, and Z. Vager†
Argonne National Laboratory, Argonne, Illinois 60439
(Received 18 February 1977)

Excitation functions of the total proton and α-particle yields from the $^{12}C + ^{16}O$ reaction have been measured in the range $E_{c.m.} = 12.9$ to 27.4 MeV, with angular distribution measurements at $E_{c.m} = 14.9$, 21, and 26.6 MeV. For comparison, the elemental distribution of evaporation residues was also measured at the latter three energies. The α excitation curve exhibits structure corresponding to the oscillations seen in an earlier measurement of the total fusion cross section, while the proton cross section increases rather smoothly with energy. At 15 MeV all the proton and α cross section is accounted for by the observed evaporation residues, but an increasing excess of light-ion production is seen at the higher energies. The excess cross section, if interpreted as 3α production, compensates for the previously observed decrease in fusion cross section below the expected total reaction cross section.

[NUCLEAR REACTIONS $^{12}C(^{16}O,p)$, $^{12}C(^{16}O,\alpha)$, $E_{lab} = 30-64$ MeV, measured $\sigma(\theta,E)$; $^{12}C(^{16}O,x)$, $E_{lab} = 35$, 49, 62 MeV, measured $\sigma(\theta,Z)$.]

I. INTRODUCTION

A recent study[1] of the complete fusion of the $^{16}O + ^{12}C$ system has revealed the presence of oscillations in the cross section for compound nucleus formation as a function of incident energy. A subsequent investigation[2] has shown that similar oscillations in the fusion cross section σ_{fus} appear in the $^{12}C + ^{12}C$ system but not in the $^{18}O + ^{12}C$ or $^{19}F + ^{12}C$ systems.

Another interesting feature which is exhibited by these systems, as well as others,[3] is the behavior of the fusion cross section relative to the total reaction cross section. At lower bombarding energies fusion dominates the reaction cross section, but at higher energies fusion represents a decreasing fraction of the total reaction cross section σ_R. Glas and Mosel[4] have shown that this behavior is expected if fusion is limited by the Coulomb barrier at low energies and by a critical radius (beyond which fusion cannot occur) at higher energies.

To further elucidate such features of the heavy-ion fusion process, we have initiated a study of the charged light ions (i.e., protons and α particles) emitted from these colliding systems—a measurement complementary to the previous work. A search for structure in the proton and α-particle excitation functions can provide information concerning the source of oscillations in σ_{fus}. It is also instructive to compare the absolute p and α production cross sections, σ_p and σ_α, with the light-ion yield implied by the observed fusion cross section, especially at higher energies where σ_{fus} saturates.

The first system studied and the subject of this report is $^{16}O + ^{12}C$. In the spirit of the fusion study, attention was focused on the total light-ion cross sections rather than on processes leading to specific final states. Excitation curves and several angular distributions were measured for the proton and α-particle yields.

In addition, it is necessary to know the fusion cross section as a function of atomic number of the residual nuclei σ_z in order to make a quantitative comparison of σ_p, σ_α, and σ_{fus}. Hence we have measured σ_z at several beam energies with an E-ΔE telescope using a gas ionization counter to provide the dE/dx information with resolution adequate to resolve the elements.

II. EXPERIMENTAL METHOD

Beams of 30 to 64 MeV ^{16}O ions from the Argonne National Laboratory tandem accelerator were incident on self-supporting ^{12}C targets of 20 to 40 $\mu g/cm^2$ areal density.

Two ΔE-E counter telescopes were employed to detect and identify the light reaction products. Telescope 1 used silicon surface-barrier detectors of 15 and 2000 μm thickness, while 7.2 and 1500 μm thick detectors were used in telescope 2. The ΔE and E pulses were digitized and stored in a two-parameter array in the PDP-11 computer memory for each telescope.

Protons and α particles completely dominated the spectra and were well resolved from each other. Very few events were observed with other values of MZ^2 below that of ^{12}C. Those particles which stopped in the ΔE detectors with an energy deposit of more than 1 MeV were counted as α particles, but only protons which reached the E detectors were included in determining the proton cross section. Some distortion of the high energy

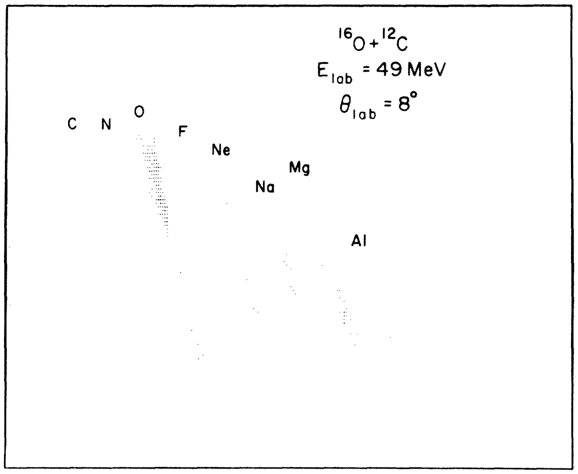

FIG. 1. A contour plot of heavy evaporation residues. Signal amplitude from the gas ionization ΔE detector is graphed along the x axis, and E signal height along the y axis.

proton spectra was observed because the E detectors could not stop the most energetic protons (> 18 MeV). This did not significantly affect the integration of the spectrum. A small hydrogen contamination in the target yielded a sharp proton-knockout peak which was subtracted before integration.

An excitation curve of σ_α and σ_p was measured in steps of 0.5 to 2.0 MeV in the range E_{lab} = 30–64 MeV. For this measurement, telescope 1 was positioned at $\theta_{lab} = 15°$ and telescope 2 at $\theta_{lab} = 25°$. In order to determine total cross sections, complete angular distributions were measured at E_{lab} = 35, 49, and 62 MeV. Telescope 1 was used to measure the angular distribution in the range $\theta_{lab} = 10°–90°$ while telescope 2 was used in the range $\theta_{lab} = 90°–170°$.

A ΔE-E counter telescope similar to that described by Fowler and Jared[5] was used to detect the evaporation residues. A gas ionization chamber provides the dE/dx signal and a silicon surface-barrier detector is mounted inside the gas volume to give the E signal. This design uses only one window of about 50 $\mu g/cm^2$ thickness. The density of gas (10% CH_4-90% Ar) was about 0.5 mg/cm^2 along the flight path.

The E and ΔE signals were digitized and stored in a 256 × 128-channel array in the computer. The events corresponding to a particular Z were projected out of this array using a two-parameter window and integrated. A typical ΔE-E spectrum is shown in Fig. 1 to illustrate the Z resolution provided by this detector.

To determine σ_z angular distributions of the evaporation residue yields were measured from $\theta_{lab} = 3°$ to 30° in steps of 1° to 3° at laboratory energies of 35, 49, and 62 MeV.

III. RESULTS

Some representative α-particle spectra measured for the excitation curve are shown in Fig. 2. As a means of displaying the data, the number

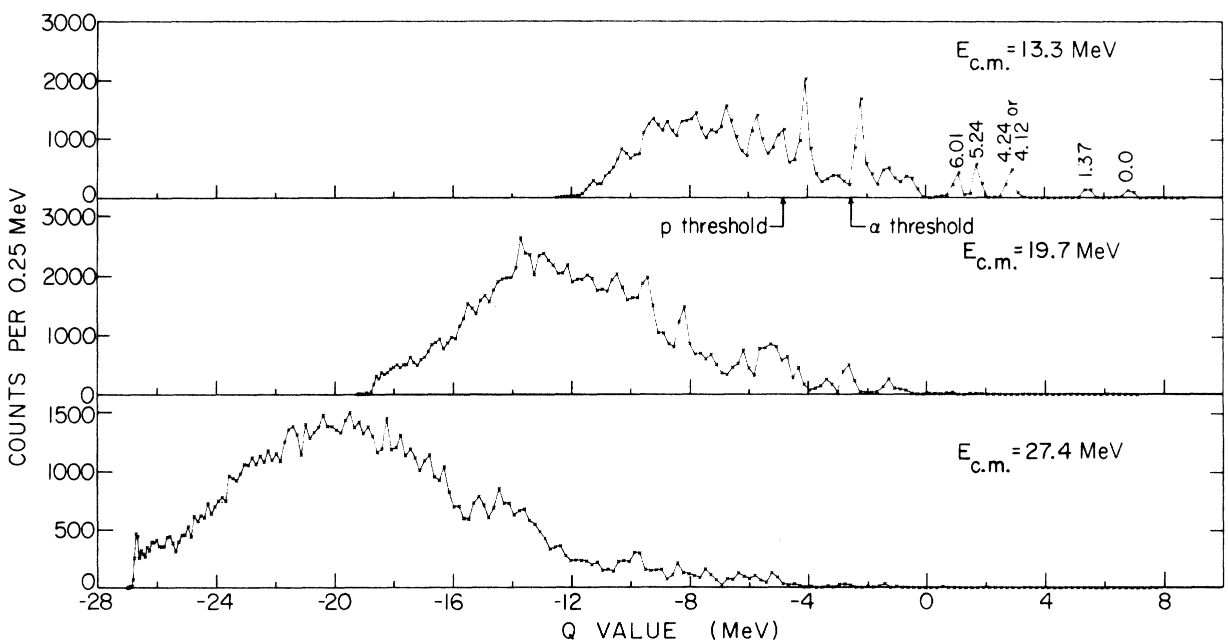

FIG. 2. Spectra of α particles at the indicated beam energies at $\theta_{lab} = 15°$. The α energies have been transformed into their Q values in an assumed $^{12}C + ^{16}O \rightarrow ^{24}Mg + \alpha$ reaction.

of counts is graphed as a function of Q value in an assumed $^{24}Mg+\alpha$ final state. Of course, some of the α yield comes from final systems involving more than two nuclei, for which this transformation is not valid. The first few levels in ^{24}Mg are labeled in Fig. 2 for orientation purposes. Population of the low-lying levels in ^{24}Mg decreases at higher bombarding energies and the α-particle energy spectrum shifts to more negative Q values.

Examples of angular distributions of the total α and proton yields are shown in Fig. 3. Particle yields have been integrated over their kinetic energy spectra. The absolute normalization of the cross section was determined by a comparison between forward-angle elastic scattering and predictions of the optical model using previously determined parameters[6] ($V_0 = 7.5$ MeV $+ 0.4E_{c.m.}$, $W_0 = 0.4$ MeV $+ 0.125E_{c.m.}$, $R_0 = R_{I_0} = 1.34$ fm, and $a = a_I = 0.45$ fm). The shapes of these angular distributions change little with bombarding energy.

The α-particle and proton total cross sections (integrated over emission angle and energy), σ_α and σ_p, are graphed as a function of incident energy in Fig. 4. To produce these curves, the differential cross sections, which were measured as a function of bombarding energy, were converted into total cross-section values by normalization

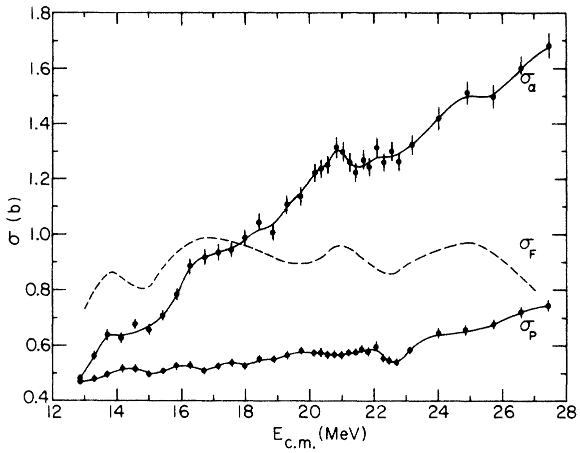

FIG. 4. Excitation curves of total α and proton yield. Lines are drawn only to guide the eye. The smooth line through the fusion cross section data of Ref. 1 is reproduced here as a dashed line.

factors interpolated between the energies at which angular distributions were measured. Interpolation of the normalization factors is justified by the fact that they change less than 10% between 35 and 62 MeV.

Relative uncertainties in the excitation curves can be estimated by comparing the two or three independent measurements made at 17 energies. The standard deviation of these values is 3% for both σ_α and σ_p. The absolute uncertainty in the cross sections is estimated to be about 7%.

Angular distributions of the evaporation residues at $E_{c.m.} = 21$ MeV are shown in Fig. 5. If the residues have a roughly Gaussian distribution in θ for each mass, then a plot of $\ln(d\sigma/d\Omega)$ as a function of θ^2 (as in Fig. 5) should approximate a straight line. Indeed, this is true of σ_{Si}, σ_{Al}, and σ_{Na} in the figure. However, σ_{Mg} and σ_{Ne} approximate two straight line segments. The steep portion of the curve probably corresponds to $2p$ emission, while the nuclei which reach larger angles may result from α emission in the case of Mg. For Ne the two lines probably represent α, $2p$, and 2α emission. The fact that the lines, in this hypothesis, corresponding to α and 2α emission have about the same slope is not inconsistent. More energetic α particles must be emitted to reach particle-stable states in Mg than those involving 2α evaporation.

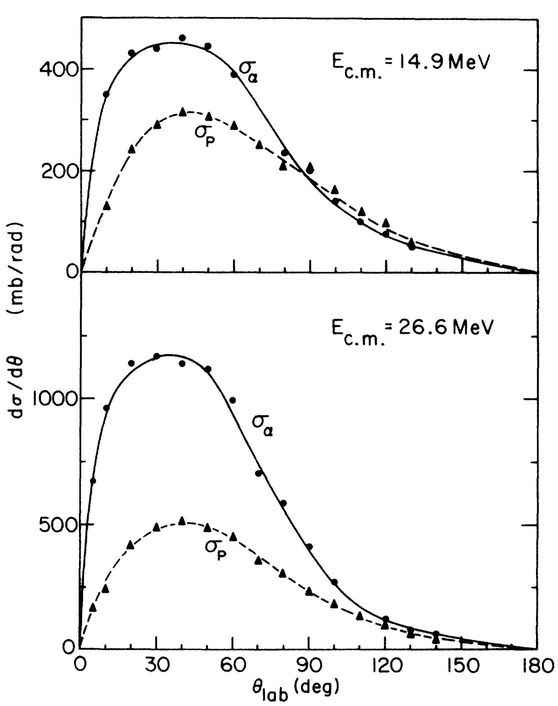

FIG. 3. Angular distributions of α particles σ_α and protons σ_p at the indicated beam energies. Note that $d\sigma/d\theta = 2\pi \sin\theta(d\sigma/d\Omega)$ is graphed so that the area under the curve is σ. Lines are drawn only to guide the eye.

Total cross sections for the production of each element were calculated by integration of the angular distributions and are listed in Table I. The absolute cross sections were determined by a comparison with forward-angle elastic scattering and have an estimated uncertainty of 7%. The ele-

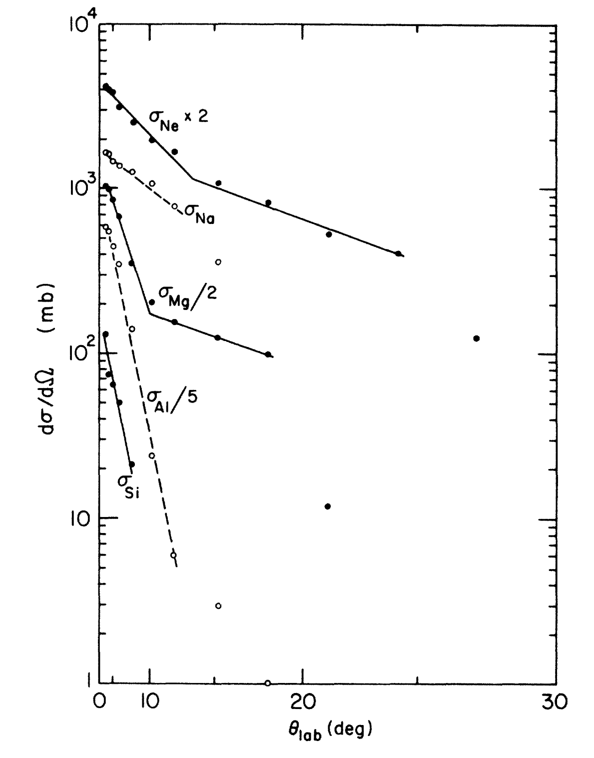

FIG. 5. Angular distributions of the evaporation residues at $E_{c.m.} = 21$ MeV. The ordinate is proportional to $\ln(d\sigma/d\Omega)$ and the abscissa to $\theta_{lab}{}^2$. The straight lines on the graph are discussed in the text.

mental fusion cross sections σ_Z are also displayed in Fig. 6(a). All nuclei detected with Z greater than the projectile were included in determining the fusion cross section. With increasing energy the Al and Si cross sections decrease, while those for lighter elements increase.

Table I includes a comparison of σ_Z with results of two other recent measurements at a nearby energy. The experiment of Weidinger *et al.*[7] was similar to the present one except that time of flight was also measured to determine mass as well as charge of the evaporation residues. The elemental cross sections of Ref. 7, summed over their isotopic decomposition, agree very well with the present results. Kotata *et al.*[8] have measured the intensities of γ rays emitted by the evaporation residues to determine the production cross sections for individual nuclides. Their results were also summed over neutron number for inclusion in Table I. The agreement with the present results is not as good, particularly for Ne, Al, and Mg. As mentioned in Ref. 8, some of this difference could be due to an unresolved ^{23}Na line near the ^{20}Ne $2^+ \rightarrow 0^+$ γ ray and to direct population of ground states or high energy γ transitions to ground states.

TABLE I. A summary and comparison of heavy- and light-ion cross sections.

$E_{c.m.}$ (MeV)	15.0	21.0	26.6	26.0[a]	26.0[b]
σ_F (mb)	0	0	5		
σ_{Ne} (mb)	221	380	323	271	511
σ_{Na} (mb)	150	239	254	274	237
σ_{mg} (mb)	164	188	222	219	158
σ_{Al} (mb)	220	141	72	82	40
σ_{Si} (mb)	10	5	5		
σ_{fus} (mb)	765	952	881	870	946
$\Sigma\sigma_Z \Delta Z$ (e mb)	1882	2754	2595		
σ_p (mb)	495	566	721		
σ_α (mb)	657	1297	1601		
$\sigma_p + 2\sigma_\alpha$ (e mb)	1809	3160	3923		
$\sigma_{3\alpha}$ (mb)	0	68	221		
$\sigma_{reaction}$ (mb)	835	1100	1240		

[a]Reference 7. [b]Reference 8.

IV. CONCLUSIONS

The trend of the fusion cross section[1] is reproduced in Fig. 4 for comparison with the light-ion yields. A correspondence between fluctuations in the excitation functions of σ_{fus} and σ_α is evident from this figure. On the other hand, σ_p exhibits little structure. Hence the evaporation channels involving α-particle emission must be responsible for the oscillations in σ_{fus}. It should be pointed out that the oscillations in σ_α are features of the inte-

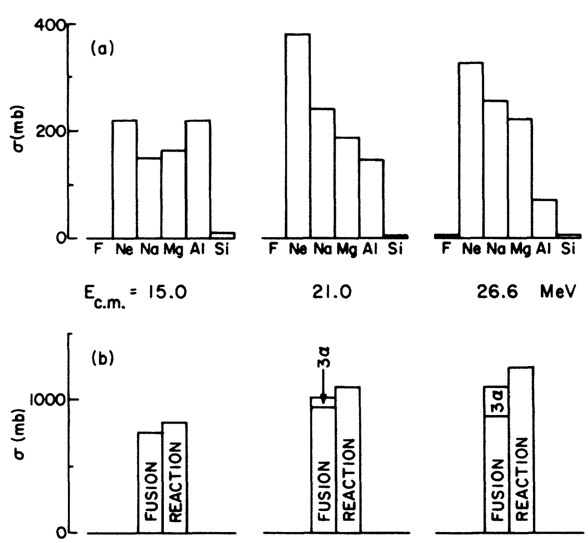

FIG. 6. (a) Elemental distribution of the fusion cross section at the indicated beam energies. (b) Comparison of the fusion cross section with the expected total reaction cross section at the same beam energies. The additional cross section labeled "3α" is discussed in the text.

grated cross section and are not localized to a specific discrete state or small group of states. Nor are they localized to one region of Q value.

The elemental decomposition of σ_{fus} in Fig. 6(a) also provides information on the structure in σ_{fus}. Although the general behavior of σ_Z indicates an increasing number of particles evaporated with increasing energy, the Ne cross section is an exception. It shows a peak at 21 MeV where σ_{fus} peaks. Based on these three energies, it appears that the Ne cross section is strongly correlated with at least some of the oscillations in σ_{fus}.

Structure in the excitation curve of $^{16}O+{}^{12}C$ fusion has also been observed in measurements[8-10] of γ rays emitted by evaporation residues. The fluctuations seen in the γ-ray measurements are generally in agreement with the results of Ref. 1 and the present work. There appears to be additional structure near $E_{c.m.}=22$ MeV (an energy region not fully investigated in Ref. 1), as has been pointed out in Refs. 8 and 9. Only Ref. 8 has calculated total fusion cross sections from γ-ray measurements which can be quantitatively compared with the results of Ref. 1. The most notable disagreement in these results is at $E_{c.m.} < 19$ MeV, where the charged particle measurements are about 100 mb larger than the γ-ray results. The nature of the disagreement is not known at present. However, when making such detailed comparisons it must be remembered that the detection of evaporation residues, γ rays, and light ions measure somewhat different things and have different uncertainties which must be taken fully into account before drawing any conclusions about fusion cross-section behavior.

It is evident from Refs. 8 and 9 that the most pronounced fluctuations occur in the ^{24}Mg cross section at lower incident energies and in the ^{20}Ne cross section at higher energies. The channels involving nucleon emission are rather smooth. This is in agreement with the observation of structure in σ_α but not in σ_p. Since the oscillations are strongest in the α and 2α emission processes, it is possible that high entrance partial waves are responsible for the structure.

A striking difference between light- and heavy-ion emission can also be seen in Fig. 4. σ_p increases slowly and σ_α increases rapidly with beam energy, while σ_{fus} saturates and perhaps even falls at higher energies. Some increase in light-ion yield can be attributed to increased evaporation multiplicities, but the deviation appears larger than this.

The comparison of absolute yields can be quantified by invoking charge conservation. For each Al ion produced, one unit of charge must have evaporated from the compound system. For each Mg ion, two units of charge were evaporated. In general, the total charge cross section evaporated is $\sum(14-Z)\sigma_Z$. Each proton accounts for one unit of charge evaporated, and each α particle for two units. The comparison is convenient because it does not require mass measurements or neutron detection. There are, however, other sources of light ions not included in the charge balance. One example is inelastic excitation of ^{12}C to particle-unbound levels, leading to its breakup into three α particles. Another is 3α emission from the compound nucleus. Although the latter is a fusion-evaporation process, it could not be distinguished from inelastic processes and was not included in the determination of σ_{fus}. Hence charge balance becomes an inequality:

$$\sum_{Z=9}^{13}(14-Z)\sigma_Z \leq \sigma_p + 2\sigma_\alpha \ .$$

Some values for this relation are listed in Table I. At 15 MeV equality holds within experimental uncertainty; i.e., all the light ions are accounted for by evaporation leading to the observed final nuclei. For higher energies, an excess of light ions appears and grows with bombarding energy. Hence the processes leading to light-ion emission continue to increase with energy, unlike σ_{fus}.

If the excess light-ion charge balance comes from either of the previously listed processes involving 3α emission, the extra cross section can be calculated. Since 3α emission liberates six units of charge:

$$\sigma_{3\alpha} = \tfrac{1}{6}\left[\sigma_p + 2\sigma_\alpha - \sum_{Z=9}^{13}(14-Z)\sigma_Z\right].$$

The value of $\sigma_{3\alpha}$ is also tabulated in Table I.

A rather interesting result is obtained by adding $\sigma_{3\alpha}$ to σ_{fus}, as shown in Fig. 6(b). The sum increases with energy and remains a constant and relatively large fraction of the reaction cross section calculated in the optical model, unlike σ_{fus} alone. It remains to be determined whether $\sigma_{3\alpha}$ is really a part of the fusion cross section or represents other reaction processes. Even if $\sigma_{3\alpha}$ arises from 3α evaporation, its addition to σ_{fus} would not damp the previously observed oscillations, because σ_α fluctuates in phase with σ_{fus}.

We are grateful to Mr. Kasra Daneshvar for his assistance in fabrication of the gas-ionization counter.

*Work performed under the auspices of the U.S. ERDA, Division of Physical Research.

†Present address: Department of Nuclear Physics, The Weizmann Institute of Science, Rehovot, Israel.

[1]P. Sperr, S. Vigdor, Y. Eisen, W. Henning, D. G. Kovar, T. R. Ophel, and B. Zeidman, Phys. Rev. Lett. 36, 405 (1976).

[2]P. Sperr, T. H. Braid, Y. Eisen, D. G. Kovar, F. W. Prosser, Jr., J. P. Schiffer, S. L. Tabor, and S. Vigdor, Phys. Rev. Lett. 37, 321 (1976).

[3]R. G. Stokstad, J. Gomez del Campo, J. A. Biggerstaff, A. H. Snell, and P. H. Stelson, Phys. Rev. Lett. 36, 1529 (1976); R. R. Betts, W. A. Lanford, M. H. Mortensen, and R. L. White, in Proceedings of the Symposium on Macroscopic Features of Heavy-Ion Collisions [Argonne National Laboratory Report No. ANL/PHY-76-2 (unpublished)], p. 443; and M. Conjeaud, S. Gary, S. Harar, and J. P. Wieleczko, *ibid.*, p. 499.

[4]D. Glas and U. Mosel, Phys. Rev. C 10, 2620 (1974).

[5]M. M. Fowler and R. C. Jared, Nucl. Instrum. Methods 124, 341 (1975).

[6]R. E. Malmin, Argonne National Laboratory Physics Division Informal Report No. PHY-1972F (unpublished).

[7]A. Weidinger, F. Busch, G. Gaul, W. Trautmann, and W. Zipper, Nucl. Phys. A263, 511 (1976).

[8]J. J. Kolata, R. M. Freeman, F. Haas, B. Hersch, and J. Gallmann, Phys. Lett. 65B, 333 (1976).

[9]Z. E. Switkowski, H. Winkler, and P. R. Christensen, Phys. Rev. C 15, 449 (1977).

[10]V. K. C. Cheng, D. L. Clark, J. J. Hall, Y. Mahmud, and S. S. Hanna, Stanford University Progress Report, 1976 (unpublished), p. 35.